*Geophys. J. R. astr. Soc.* (1978) **54**, 417–438

# Dynamical rupture process on a three-dimensional fault with non-uniform frictions and near-field seismic waves

Takeshi Mikumo and Takashi Miyatake *Disaster Prevention Research Institute, Kyoto University, Uji, Kyoto, Japan*

Received 1977 December 19; in original form 1977 July 26

**Summary.** Dynamical rupture process on the fault is investigated in a quasi-three-dimensional faulting model with non-uniform distributions of static frictions or the fracture strength under a finite shearing pre-stress. The displacement and stress time functions on the fault are obtained by solving numerically the equations of motion with a finite stress–fracture criterion, using the finite difference method.

If static frictions are homogeneous or weakly non-uniform, the rupture propagates nearly elliptically with a velocity close to that of $P$ waves along the direction of pre-stress and with a nearly $S$ wave velocity in the direction perpendicular to it. The rise time of the source function and the final displacements are larger around the centre of the fault. In the case when the static frictions are heavily non-uniform and depend on the location, the rupture propagation becomes quite irregular with appreciably decreased velocities, indicating remarkable stick–slip phenomena. In some cases, there remain unruptured regions where fault slip does not take place, and high stresses remain concentrated up to the final stage. These regions could be the source of aftershocks at a next stage.

The stick–slip faulting and irregular rupture propagation radiate high-frequency seismic waves, and the near-field spectral amplitudes tend to show an inversely linear frequency dependence over high frequencies for heavily non-uniform frictional faults.

## 1 Introduction

A number of recent studies on the earthquake source mechanism have shown that a majority of shallow earthquakes and even many deep-focus earthquakes are caused by sudden shear faulting under tectonic stresses. The application of the elastic dislocation theory (Maruyama 1963; Haskell 1964, 1969; Aki 1968) has proved powerful to model general features of the faulting process, particularly to account for seismic observations in relatively long-period ranges, as well as static deformations at least to a first approximation, although the generation of high-frequency seismic waves often observed at short distances has not been

Downloaded from http://gji.oxfordjournals.org/ at Library of Research Reactor Institute, Kyoto University on December 7, 2014

well explained. In the above dislocation models, however, some simplified assumptions are made rather arbitrarily on the process of rupture propagation over the fault plane and the displacement time function, without physical considerations into stress conditions on and around the fault. For more comprehensive understanding of the dynamical process at the source and complex ground motions in the near-field, it will be essentially important to incorporate how the rupture initiates, spreads and stops on the fault and how dynamic slip motions are developed under shearing stresses.

Another approach along this line has been to deal with the faulting process as propagating shear cracks by taking into account the initial stress field, frictions and/or cohesive forces on the fault. The first study of this kind was made by Kostrov (1966), who treated the case of unsteady propagation of longitudinal shear cracks in an infinite medium, by introducing a fracture criterion depending on the energy balance at the advancing crack tip. During the last decade since his study, dynamic crack problems have been solved analytically or numerically; in one-dimensional mass spring models (Burridge & Knopoff 1967; Dietreich 1972; Knopoff, Mouton & Burridge 1973; Ohnaka 1973); in two-dimensional in-plane and anti-plane shear cracks growing at a constant velocity or with self-similar propagation under different fracture criterions and boundary conditions (Burridge 1969; Burridge & Halliday 1971; Burridge 1973; Hanson, Sanford & Shaffer 1971, 1974; Ida & Aki 1972; Ida 1973; Takeuchi & Kikuchi 1973; Fossum & Freund 1975; Husseini *et al.* 1975; Andrews 1975, 1976; Madariaga 1976; Das 1976). Some of these authors have calculated near and far-field displacements and their spectra of seismic waves radiated from finite cracks, but the two-dimensional cracks still appear inadequate to compare the results with the observations. More realistic three-dimensional analysis has been made in finite-element models (Dietreich 1973) to get the relation between fault displacements, stress drops and rupture dimensions, and analytically for elliptical shear cracks growing steadily with subsonic speeds in an infinite pre-stressed medium (Richards 1976). A recent work of Yamashita (1976) gave numerical solutions for the rupture propagation in a three-dimensional model with frictions, which is based on a mechanical model by Otsuka (1971), being subjected to the inhomogeneous initial stress field. These three-dimensional studies, however, do not directly aim at the problem of generation of short-period waves from the fault.

In the present paper, we investigate the dynamical rupture process in a quasi-three-dimensional, frictional fault, which is somewhat similar to Yamashita's but seems slightly more complete, with the distribution of static and dynamic frictions on the fault surface and the initial shear stress, and also seismic waves radiated from the fault. We are mainly concerned here with the case of non-uniform distribution of static frictions or the fracture strength, which would be a manifestation of the irregularities of elastic property and structure involved in pre-existing fault gouge or in newly-formed fault planes. It is expected that such distributions will cause non-uniform rupture propagation and stick–slip-like phenomena as in laboratory experiments (e.g. Brace & Byerlee 1966; Brace 1972; Byerlee 1970; Johnson, Wu & Sholz 1973), which could radiate high-frequency seismic waves. For a number of possible cases, we calculate the mode of rupture propagation based on a fracture criterion, the time history of fault displacements, final slips and stress drops on each point of the fault plane, by the aid of the finite difference technique. Near-field displacements, synthetic seismograms and their frequency dependence of the amplitude spectra of the radiated seismic waves are also calculated for the various rupture processes.

## 2 Quasi-three-dimensional, frictional faulting model

We suppose that the actual rupture process on the fault may be that described below: the rupture nucleates and then initiates suddenly at a small region where gradually accumulated

Downloaded from http://gji.oxfordjournals.org/ at Library of Research Reactor Institute, Kyoto University on December 7, 2014

tectonic stresses first overcome the weakest fracture strength; this immediately yields stress concentration in the adjacent regions and produces successive slips when the concentrated stress exceeds the inherent strength there; the resulting rupture spreads rapidly over the fault and finally stops at the fault edges or in regions where the strength is higher than the stress. However, if the fracture strength and/or the initial shear stress are not homogeneously distributed, the rupture will not propagate uniformly both in space and time, and the slips might not take place over the entire fault.

The present problem may be formulated as follows. Now we consider an infinite, homogeneous elastic medium, and take the fault in the $x$–$y$ plane of a Cartesian coordinate with its origin at the nucleation point of rupture. Suppose that the initial shear stress $\sigma_0(\sigma^0_{zx}, \sigma^0_{yz})$ is applied parallel to the fault plane, making an angle $\alpha$ to the $x$ axis. The displacement components $(u, v)$ and stress components $(\sigma_{xx}, \sigma_{yy}, \sigma_{xy}, \sigma_{xz}, \sigma_{yz})$ on the fault satisfy the equations of motion, and hence we have the wave equations,

$$\left.\begin{aligned} \rho\frac{\partial^2 u}{\partial t^2} &= (\lambda+2\mu)\frac{\partial^2 u}{\partial x^2} + \mu\frac{\partial^2 u}{\partial y^2} + (\lambda+\mu)\frac{\partial^2 v}{\partial x\,\partial y} + \mu\frac{\partial^2 u}{\partial z^2} \\ \rho\frac{\partial^2 v}{\partial t^2} &= (\lambda+2\mu)\frac{\partial^2 v}{\partial y^2} + \mu\frac{\partial^2 v}{\partial x^2} + (\lambda+\mu)\frac{\partial^2 u}{\partial x\partial y} + \mu\frac{\partial^2 v}{\partial z^2} \end{aligned}\right\} \tag{1}$$

where $\lambda$ and $\mu$ are Lame's elastic constants and $\rho$ is the density of the medium. When we consider two regions occupying $z > 0$ and $z < 0$, $u$ and $v$ are discontinuous and $\sigma_{zz}$ is continuous across the plane $z = 0$, all of which should be odd functions of $z$. This implies that $u$ and $v$ tend to the half of the displacement discontinuities and $\sigma_{zz} = 0$ inside the ruptured area as $z \to 0$. It is therefore sufficient to treat the present problem in the half-space $z > 0$, because of symmetry.

Now let us solve equation (1) by the finite difference technique under the fracture criterion and the boundary conditions described later. If we denote the displacement components by $(u_{i,j}, v_{i,j})$ at the grid points $(x_i, y_j)$ $(i = 1 \sim n_x, j = 1 \sim n_y)$ on the fault plane, the second derivatives may be approximated by,

$$\left.\begin{aligned} \frac{\partial^2 u}{\partial x^2} &\cong \frac{u_{i+1,j} - 2u_{i,j} + u_{i-1,j}}{(\Delta x)^2}, \qquad \frac{\partial^2 v}{\partial x^2} \cong \frac{v_{i+1,j} - 2v_{i,j} + v_{i-1,j}}{(\Delta x)^2} \\ \frac{\partial^2 u}{\partial y^2} &\cong \frac{u_{i,j+1} - 2u_{i,j} + u_{i,j-1}}{(\Delta y)^2}, \qquad \frac{\partial^2 v}{\partial y^2} \cong \frac{v_{i,j+1} - 2v_{i,j} + v_{i,j-1}}{(\Delta y)^2} \\ \frac{\partial^2 u}{\partial x\partial y} &\cong \frac{u_{i+1,j+1} - u_{i-1,j+1} - u_{i-1,j+1} + u_{i-1,j-1}}{4\Delta x\Delta y}, \\ \frac{\partial^2 v}{\partial x\partial y} &\cong \frac{v_{i+1,j+1} - v_{i-1,j+1} - v_{i+1,j-1} - v_{i-1,j-1}}{4\Delta x\Delta y} \end{aligned}\right\}. \tag{2}$$

The shear stress components $\sigma_{zx}$ and $\sigma_{yz}$ may be written by

$$\left.\begin{aligned} \sigma_{zx} &\cong \mu(\mathrm{U} - u_{i,j})/\Delta z = \sigma^0_{zx} - \mu u_{i,j}/\Delta z \\ \sigma_{yz} &\cong \mu(\mathrm{V} - v_{i,j})/\Delta z = \sigma^0_{yz} - \mu v_{i,j}/\Delta z \end{aligned}\right\} \tag{3}$$

where the initial stresses are defined as

$$\sigma^0_{zx} \equiv \mu\mathrm{U}/\Delta z = \sigma_0\cos\alpha, \qquad \sigma^0_{yz} \equiv \mu\mathrm{V}/\Delta z = \sigma_0\sin\alpha$$

Downloaded from http://gji.oxfordjournals.org/ at Library of Research Reactor Institute, Kyoto University on December 7, 2014

$\Delta x, \Delta y$ and $\Delta z$ are the grid spacing in the $x, y$ and $z$ directions respectively, and U and V are constant slip displacements of the upper fault surface relative to a fixed coordinate. From equation (3) we have

$$\frac{\partial^2 u}{\partial z^2} \cong \frac{\sigma_0 \cos\alpha}{\mu \Delta z} - \frac{u_{i,j}}{(\Delta z)^2}, \quad \frac{\partial^2 v}{\partial z^2} \cong \frac{\sigma_0 \sin\alpha}{\mu \Delta z} - \frac{v_{i,j}}{(\Delta z)^2}. \tag{4}$$

If we write the right-hand sides in equation (1) as $F_x$ and $F_y$, which are obtained from equations (2) and (4), these correspond to the force components per unit volume applied to a mass on $(x_i, y_j)$, and can be rewritten

$$\rho \ddot{u}_{i,j} = F_x, \quad \rho \ddot{v}_{i,j} = F_y. \tag{5}$$

It would be interesting to mention here three-dimensional mechanical models which correspond to the present case. Otsuka (1971) introduced a mechanical model composed of helical and leaf springs as a static problem to simulate seismicity and its migration. His model is appropriate also in dynamic problems so long as we consider a single displacement component parallel to the applied stress as in Yamashita (1976). Our present case given by equation (1) requires a more complex model such as schematically illustrated in Fig. 1. In this model each mass is connected to four adjacent masses by springs with a given compressibility ($K$) and rigidity ($L$), and to four masses by diagonal springs with different constants ($K'$ and $L'$), and also supported vertically by a string with an appropriate rigidity ($M$). The four diagonal springs yield additional forces, which are expressed by 16 terms including $K'$, $L'$, $\Delta u_{i,j}$ and $\Delta v_{i,j}$, when compared with Otsuka's model. Rearranging these terms and using some geometrical relations between the displacements, the $x$ and $y$ components of the resultant body force applied on the $(i,j)$ mass are written by,

$$\begin{aligned} Fx \cdot V &= (K + 2K')(u_{i+1,j} - 2u_{i,j} + u_{i-1,j})/h + (L + 2L')(u_{i+1,j} - 2u_{i,j} + u_{i-1,j})/h \\ &\quad + (K' - L')(v_{i+1,j} - 2v_{i,j} + v_{i-1,j})/\sqrt{2}h + Mu_{i,j}/h \\ Fy \cdot V &= (K + 2K')(v_{i+1,j} - 2v_{i,j} + v_{i-1,j})/h + (L + 2L')(v_{i+1,j} - 2v_{i,j} + v_{i-1,j})/h \\ &\quad + (K' - L')(u_{i+1,j} - 2u_{i,j} + u_{i-1,j})/\sqrt{2}h + Mv_{i,j}/h. \end{aligned} \tag{6}$$

Comparing the above terms in equation (6) with those in equations (1) and (2), it is found that the present mechanical model is equivalent to the elastic medium now considered, if we assign the following constants to each of the springs; $K = (1 - 1/\sqrt{2})(\lambda + 2\mu)V/h$, $L = (1 - 1/\sqrt{2})\mu V/h$, $K' = \sqrt{2}(\lambda + 2\mu)V/4h$, $L' = \sqrt{2}\mu V/4h$ and $M = \mu V/h$, where $V$ is the volume of an elementary block ($V = \Delta x \cdot \Delta y \cdot \Delta z = h^2 \Delta z$).

Let us next describe the fracture criterion by which the rupture initiates and slip movements take place on the fault. There are mainly two different criteria in two-dimensional

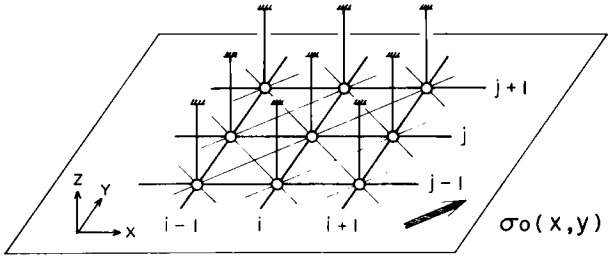


**Figure 1.** Schematic representation of the quasi-three-dimensional fault model now in consideration.

Downloaded from http://gji.oxfordjournals.org/ at Library of Research Reactor Institute, Kyoto University on December 7, 2014

crack problems: one is the conservation of a finite fracture energy at the crack tip (e.g. Kostrov 1966; Fossum & Freund 1975; Husseini *et al.* 1975), and the other is a critical comparison of shear stress with a static friction level (Burridge & Halliday 1971; Burridge 1973; and many others). The former criterion produces a well-known stress singularity at the crack tip, whereas the finite stress criterion does not account for the energy balance. In real materials, however, there should be an upper bound of shear stress that the medium can support, and it would be possible to remove the apparent mathematical singularity of the stress by introducing cohesion and/or inelastic deformation or slip-weakening into the rupture front (Andrews 1976), satisfying the finite fracture energy. It has also been shown (Das 1976) that the finite stress criterion used in numerical calculations is equivalent to a criterion based on the stress intensity factor related to energy.

For these reasons, we use a finite stress criterion similar to Burridge (1973) and others. Static and dynamic frictional stresses and the corresponding forces on the fault are defined as

$$\sigma_s = \mu_s \sigma^0_{zz}, \quad F_s = \sigma_s/\Delta z; \quad \sigma_d = \mu_d \sigma^0_{zz}, \quad F_d = \sigma_d/\Delta z \tag{7}$$

where $\sigma^0_{zz}$ is the initial normal stress, and $\mu_s$ and $\mu_d$ are the coefficients of static and dynamic frictions which are assumed to vary depending on the location but independent of time, slip and slip velocity. The criteria we use are:

(1) If the resultant force $F = \sqrt{F_x^2 + F_y^2}$ exceeds the static frictional force assigned to the location, i.e. $F \geqslant F_s$, slip immediately begins. Each point on the fault is kept stuck at the initial stage and until this condition is satisfied.
(2) Once slip starts, each element on the fault is resisted by the dynamic frictional force during the motion, that is, the accelerating force in equation (5) reduces to,

$$F_x \to F_x - F_d \cos\alpha \quad \text{and} \quad F_y \to F_y - F_d \sin\alpha. \tag{5'}$$

(3) If the resultant force becomes smaller than the total dynamic frictional force, i.e. $F < F_d$, then the fault element sticks and is subjected to a renewed static frictional force $F_s'(F_d \leqslant F_s' < F_s)$. The element can slip again later when $F \geqslant F_s'$, but otherwise sticks up to the final stage.

A boundary condition is imposed that all displacement components $u_{i,j}$ and $v_{i,j}$ at the edge ($i = 1, n_x, j = 1, n_y$) of the prescribed fault plane equal zero.

The rupture starting from a nucleation point continues to propagate spontaneously so long as the condition (1) is satisfied, and stops at the fault edges or by the condition (3). Since the rupture front is specified at every time step by the above conditions, its propagation velocity will be determined without any other assumptions. The stresses at every point on the fault are calculated from the right-hand side of equation (5) as a function of time. The time history of the displacements are derived successively by solving equation (5') through the finite difference scheme,

$$\left.\begin{aligned} u_{t+\Delta t} &= 2u_t - u_{t-\Delta t} + (F_x - F_d \cos\alpha)(\Delta t)^2/\rho \\ v_{t+\Delta t} &= 2v_t - v_{t-\Delta t} + (F_y - F_d \sin\alpha)(\Delta t)^2/\rho \end{aligned}\right\} \tag{8}$$

and hence the rise time of the displacement function is directly estimated. The distribution of the final displacements and stresses and stress drops will be determined by this procedure. Thus, all rupture process on the present model will be completely specified by the distribution of static and dynamic frictional stresses $\sigma_s$ and $\sigma_d$ and the initial stress $\sigma_0$, or by the fracture strength $\sigma_s - \sigma_0$ and the effective stress $\sigma_s - \sigma_d$ as defined in Yamashita (1976). A dimensionless factor $\mathscr{S} = (\sigma_s - \sigma_0)/(\sigma_0 - \sigma_d)$ or $1 + \mathscr{S} = (\sigma_s - \sigma_d)/(\sigma_0 - \sigma_d)$ may also be

Downloaded from http://gji.oxfordjournals.org/ at Library of Research Reactor Institute, Kyoto University on December 7, 2014

used as an alternative indication for rupture initiation (Andrews 1976; Das 1976). It is to be remarked here that the present model is quasi-three-dimensional in the sense that the medium is bounded above by a fixed boundary from which no energies are emitted outside. This implies that the absolute values of the calculated parameters will be somewhat different from those in a completely infinite medium. The present model could easily be extended to incorporate more layers above the fault plane, if we had sufficient computer storage.

## 3 Numerical calculations

Numerical calculations are made for the various cases described below, in which intrinsic length and time scales are used, instead of introducing scaling factors, to compare the results directly with observations. $P$ and $S$ wave velocities in the medium are taken to be $V_P$ = 5.5 km/s and $V_S$ = 3.2 km/s, respectively, and the density is taken as $\rho = 2.75$ g/cm$^3$, which give $\lambda = 2.686 \times 10^{11}$ dyne/cm$^2$ and $\mu = 2.816 \times 10^{11}$ dyne/cm. These values are typical ones for granitic rocks in the upper crust.

In the finite difference equations, we have to choose appropriate values for the space dimension $h(= \Delta x = \Delta y)$ and the time increment $\Delta t$ so as to satisfy the stability condition $\Delta t < h/V_p$, otherwise the solution will be insignificant due to some instability of short-period waves and dispersion. We have tested a number of cases but the following three cases are adopted; $h = 0.25$ km, $2L = 2W = 10$ km and $\Delta t = 0.025$ s; $h = 0.5$ km, $2L = 2W = 20$ km and $\Delta t = 0.05$ s; and $h = 1.0$ km, $2L = 2W = 40$ km and $\Delta t = 0.10$ s. For all the cases, we have a 40 × 40 grid size and $V_p \Delta t/h = 0.55$.

In the present quasi-three-dimensional model, we introduce $\Delta z$ into equations (3), (4) and (5) to approximate $\partial^2 u/\partial z^2$ and $\partial^2 v/\partial z^2$, which may be regarded as the distance between the fault plane and a hypothetical fixed coordinate taken upward in the $z$ direction, as shown in Fig. 1. To estimate a reasonable range of $\Delta z$, we made preliminary calculations to get the displacements just above the fault plane in an infinite medium by applying the dynamic dislocation theory (Haskell 1969). Fig. 2 shows the displacement component parallel to the dislocation of 1 m with a rise time of 3 s, which spreads radially with a constant velocity of 3.2 km/s, where $t$ is the time elapsed after the rupture initiation and $x$ and $z$ are the distances of the observation points measured parallel and perpendicular to the fault. It is noticed that the calculated displacements at every time step decrease rapidly within distances of 1.0–1.5 km. Some undulations in the curves around $z$ = 1.5–2.5 km may be due to interferences of the waves emitted from the initiation point of rupture and from the fault portion just below the observation point. From this result, it may be

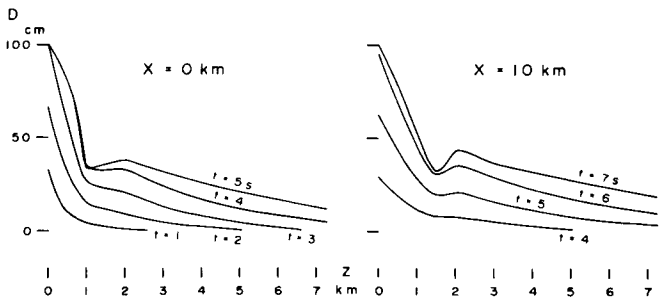


**Figure 2.** Dynamic displacements at short distances close to the fault surface, where $X$ and $Z$ are measured parallel and perpendicular to the fault from the point of rupture initiation, and $t$ is the elapsed time. For other parameters, see text.

Downloaded from http://gji.oxfordjournals.org/ at Library of Research Reactor Institute, Kyoto University on December 7, 2014

reasonable to adopt $\Delta z = 1.0$–$1.5$ km to approximate the second derivatives of the displacements at $z = 0$, and we take the average of 1.2 km for its final value.

We are particularly interested in the non-uniform distribution of the fracture strength on the fault. There is some evidence that the distribution of the strength of rock material is approximated by the Weibull's distribution with two specific coefficients, which is not far from a normal random distribution (Miyatake 1977). For this reason, we assume here that static frictional stresses are distributed two-dimensionally in a normal random fashion around a certain average with some standard deviations. In most of the present calculations, the minimum value and the deviation are taken as 200 and 0–30 bar, respectively. In some special cases, however, extremely high frictions reaching 600 bar are assigned to several limited places or relatively wide regions, which may correspond to relatively large geological heterogeneities in the fault. These portions are made arbitrarily by raising up the distributed frictions that exceed a certain limit ($C_a$) by a finite ratio ($C_p$), where $1 - C_a$ is an indicator of the areal ratio of the high frictional inclusion.

Dynamic frictional stresses could also vary slightly from place to place, but are assumed here to be constant over the fault plane. Although there is some evidence from laboratory experiments (Byerlee 1970) indicating that $\mu_d/\mu_s = 0.8$ for granite, we tentatively assign 100 bar to $\sigma_d$ in most cases, which corresponds to the ratio of 0.5. Under this assumption, the effective stress $\sigma_s - \sigma_d$ also varies depending on the location. $F_s'$, a renewed static frictional force after the fault slip has been assumed to be slightly above $F_d$. In the present case, we assume that the initial shear stress is uniformly applied on the fault, although there could be a gradually varying distribution as has been treated in some cases (Yamashita 1976) and again tested in a separate paper (Miyatake 1977) or some concentrated distribution resulted from previous earthquakes (Andrews 1975). Since it is reasonable to consider the case $\sigma_d < \sigma_0 < \sigma_s$, we take various values between 155 and 198 bar for $\sigma_0$, which gives 1.02–2.90 for $1+\mathscr{S}$.

In the present model, a nuclear length or nuclear surface elements are required to start spontaneous propagation of rupture, although the propagation thereafter is prescribed by the fracture criterion. In most cases, we take $N_c = 1$ or $2L_c/h = 2W_c/h = 1$ and $N_c = 5$ or $2L_c/h = 2W_c/h = 3$, but for the case of uniform distribution of static frictions we choose $N_c = 11$ corresponding to $2L_c/h = 5$ and $2W_c/h = 3$. The implication of $L_c$ and $W_c$ in this case is somewhat different from the critical crack length in two-dimensional crack problems.

We have made a number of calculations with various combinations of the above parameters to see how sensitively the rupture process is affected, but we will discuss seven representative cases among them in the next section. The parameters specifying these cases are given in Table 1. In these calculations, there is a problem of stress singularity including numerical accuracy of the calculated stress, as in two-dimensional shear cracks. In numerical calculations for the two-dimensional case, the stress singularity has been avoided by using Irwin's fracture criterion (Das 1976). It will be demonstrated in a separate paper (Miyatake 1977) that the criterion can also be applied to Otsuka's mechanical model, which is nearly equivalent to our three-dimensional fault model, and hence that the above problem may not be serious here.

## 4 Mode of rupture propagation, source time function, and distribution of final displacements and stresses

In this section, the main results obtained from the present frictional faulting model are described. Before getting into the studies described below, we made several numerical experiments to examine the rupture patterns for different choices of the grid spacing under

Downloaded from http://gji.oxfordjournals.org/ at Library of Research Reactor Institute, Kyoto University on December 7, 2014

Downloaded from http://gji.oxfordjournals.org/ at Library of Research Reactor Institute, Kyoto University on December 7, 2014



**Table 1.** Parameters specifying frictional fault models.

| Case | $2L \times 2W$ | $\sigma_{s(min)}$ | $\sigma_{s(max)}$ | $\Delta\sigma_s$ | $C_a$ | $C_p$ | $\sigma_d$ | $\sigma_o$ | $\sigma_s-\sigma_o$ | $\sigma_s-\sigma_d$ | $N_c$ |
|---|---|---|---|---|---|---|---|---|---|---|---|
| A | 40 × 40 | 200 | 326 | 20 | | | 100 | 198 | 2–128 | 100–226 | 1 |
| B1 | 40 × 40 | 200 | 591 | 20 | 0.88 | 1.80 | 100 | 198 | 2–397 | 100–491 | 1 |
| B2 | 40 × 40 | 200 | 657 | 20 | 0.90 | 2.00 | 100 | 198 | 2–459 | 100–557 | 1 |
| C | 40 × 40 | 200 | 591 | 20 | 0.85 | 1.80 | 100 | 198 | 2–397 | 100–491 | 1 |
| F0 | 20 × 20 | 200 | 200 | 0 | | | 100 | 155 | 45 | 100 | 11 |
| F1 | 20 × 20 | 200 | 609 | 20 | 0.85 | 1.80 | 100 | 180 | 20–429 | 100–509 | 5 |
| F2 | 20 × 20 | 200 | 677 | 25 | 0.90 | 2.00 | 100 | 190 | 10–487 | 100–577 | 5 |

*Remarks:*

| | |
|---|---|
| $2L \times 2W$ | fault dimension in km |
| $\sigma_{s(min)}$ | minimum static frictional stress |
| $\sigma_{s(max)}$ | maximum static frictional stress |
| $\Delta\sigma_s$ | standard deviation (variance) of static frictional stress |
| $C_a$ | a finite level above which all static frictions are raised up to make unusual high frictions (see text) |
| $C_p$ | a multiplication factor to make the high frictions |
| $\sigma_d$ | dynamic frictional stress |
| $\sigma_o$ | initial shear stress |
| $\sigma_s-\sigma_o$ | fracture strength |
| $\sigma_s-\sigma_d$ | effective stress |
| $N_c$ | initial rupture elements |

All stresses are given in bars.

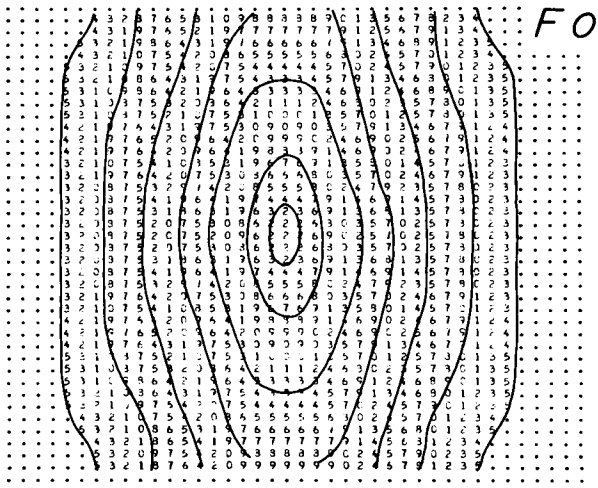


**Figure 3.** Rupture fronts at every 0.5 s after the initiation in Case F0; fault dimension 20 × 20 km.

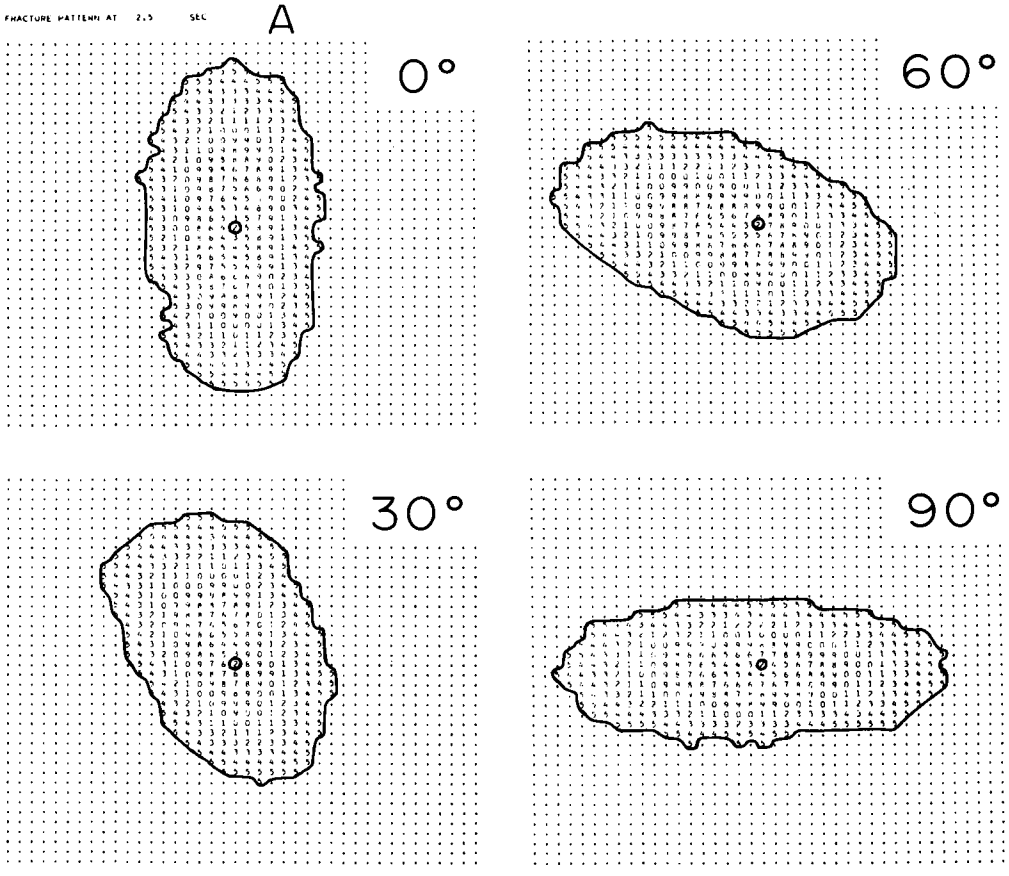


**Figure 4.** Rupture propagation in the case when the initial shear stress is applied in different directions. Case A with weakly non-uniform frictions; fault dimension 40 × 40 km.

Downloaded from http://gji.oxfordjournals.org/ at Library of Research Reactor Institute, Kyoto University on December 7, 2014

the same condition for the other parameters. The results show that the rupture pattern does not change if we choose the spacing in the range mentioned in the foregoing section. This may also be explained by the other results (Miyatake 1977) that the calculated stress intensity factor (Das 1976) was independent of the choice of the grid spacing.

Now we discuss the mode of rupture propagation in the cases of uniform and weakly irregular distribution of static frictional stresses on the fault. Fig. 3 shows the rupture front at every 0.5 s up to 2.5 s after its initiation in Case F0. It is immediately noticed that the velocities of the propagating rupture front along the longer and shorter axes are close to $P$ wave velocity and slightly less than $S$ wave velocity, respectively. Fig. 4 indicates how the rupture front extends when the initial shear stress is applied in different directions in Case A. The direction ($\alpha$) indicated on the right top is measured counterclockwise from the $x$ axis pointing downward in the figure. These four patterns clearly indicate that the direction of the longer axis tends to be parallel to that of the applied initial stress and that the propagation velocities are similar to the case in Fig. 3. Thus, it may be well established from Figs 3 and 4 that the rupture propagates almost elliptically with a velocity close to that of $P$ waves along the direction parallel to the initial shear stress and with a nearly $S$ wave

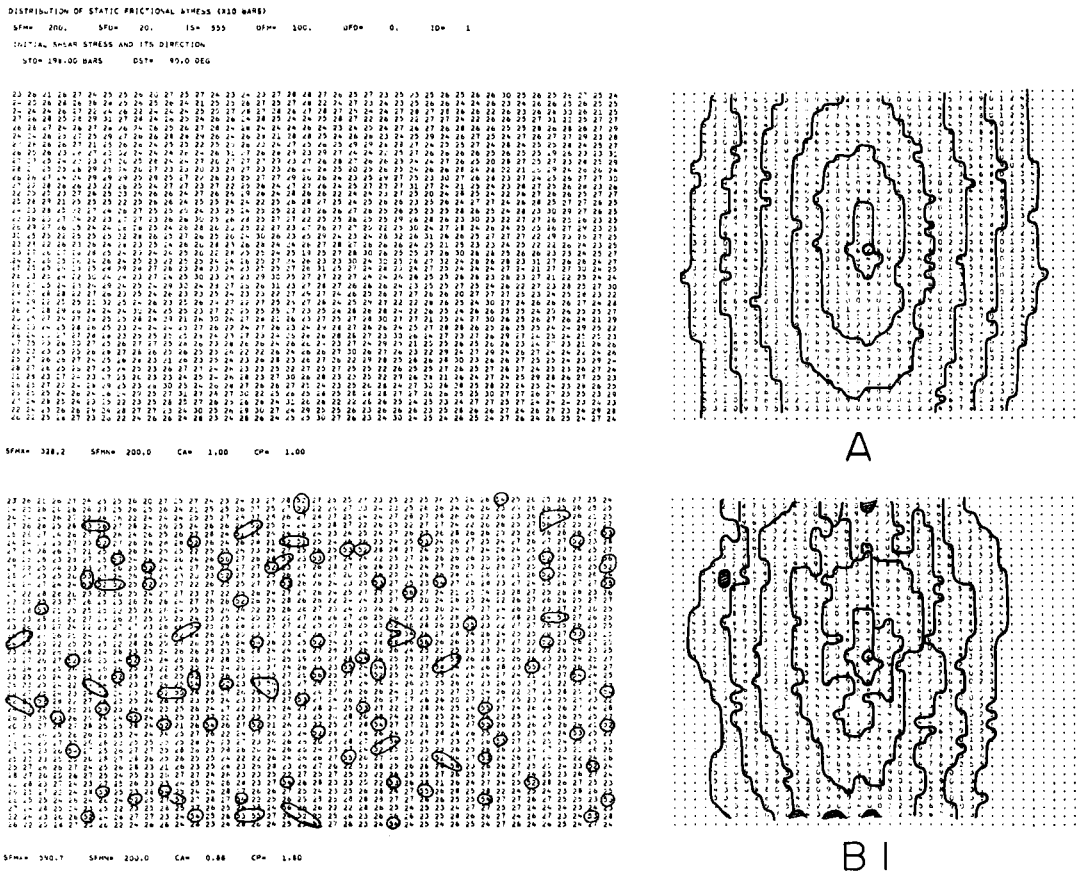


**Figure 5(a)**

**Figure 5.** Distribution of static frictional stress on the fault (left) and the corresponding rupture patterns (right). The encircled portions (left) are assumed to have unusually high frictional stress, and small shaded areas are unruptured regions. The initial stress is applied downward in the figure. Case A does not include unusual high frictions. (a) Cases A and B1, (b) Cases B2 and C.

Downloaded from http://gji.oxfordjournals.org/ at Library of Research Reactor Institute, Kyoto University on December 7, 2014

velocity in the direction perpendicular to it, when static frictions are uniformly distributed or weakly irregular on the fault surface. For two-dimensional self-similar in-plane shear cracks, it has been suggested analytically that the crack speed could reach $P$ wave velocity for weak static friction level (Burridge 1973), and also numerically shown that the velocity could change from sub-Rayleigh to super-shear and approach $P$ wave velocity as functions of the initial crack length $L_c/L$ as well as of the stress jump factor $\mathscr{S}$ (Andrews 1976; Das 1976). Our findings from a three-dimensional model partially support their results and appear to add an important conclusion that the rupture spreads at different velocities in different directions with respect to the direction of the initial stress.

The next two figures, Fig. 5(a) and (b), show four examples of the mode of rupture propagation (right side) from different distributions of static frictions on the fault (left side). The direction of the initial stress has been fixed here ($\alpha = 0°$). In Case A static frictions are not so heavily non-uniform, but Cases B1, B2 and C include a number of places with unusually high frictions within the encircled portions. We suppose that there could be this type of local geological irregularity on the fault. The rupture fronts are drawn here at every 2 s for Case C and at every 1 s for the other cases. It is clear that the shape of the rupture front becomes gradually deformed from an ellipse and its propagation velocity appreciably decreases as the high friction inclusion increases. Small shaded areas in these patterns remain unruptured up to the final stage, resisting stress concentration because of extremely high fracture strength. Ordinary normal-random distribution of static frictions

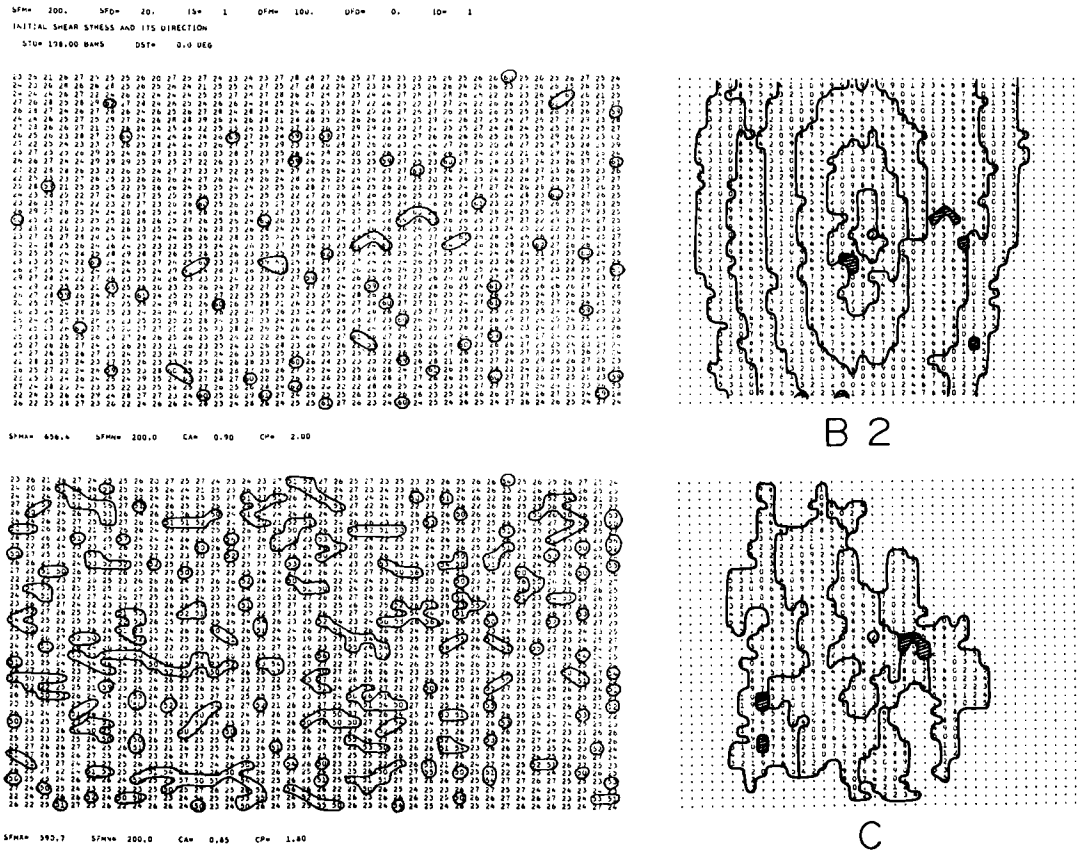


**Figure 5 (b)**

Downloaded from http://gji.oxfordjournals.org/ at Library of Research Reactor Institute, Kyoto University on December 7, 2014

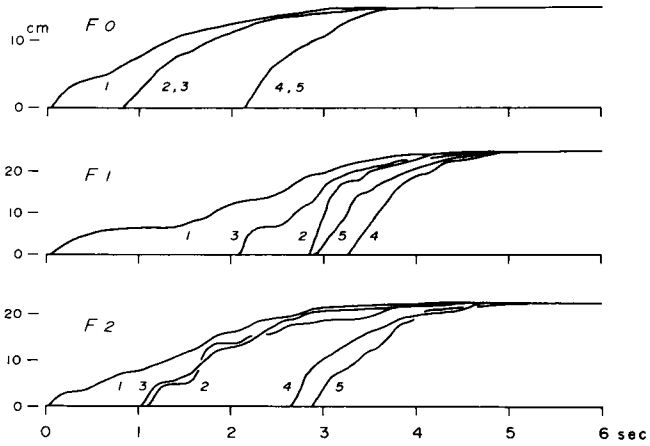


**Figure 6.** Displacement–time functions at several selected points on the fault. Cases F0, F1 and F2, where numerals beside the curves indicate the coordinate of the points. 1, $X = 10$, $Y = 10$; 2, $X = 5$, $Y = 10$; 3, $X = 15$, $Y = 10$; 4, $X = 10$, $Y = 5$; 5, $X = 10$, $Y = 15$ (units in km).

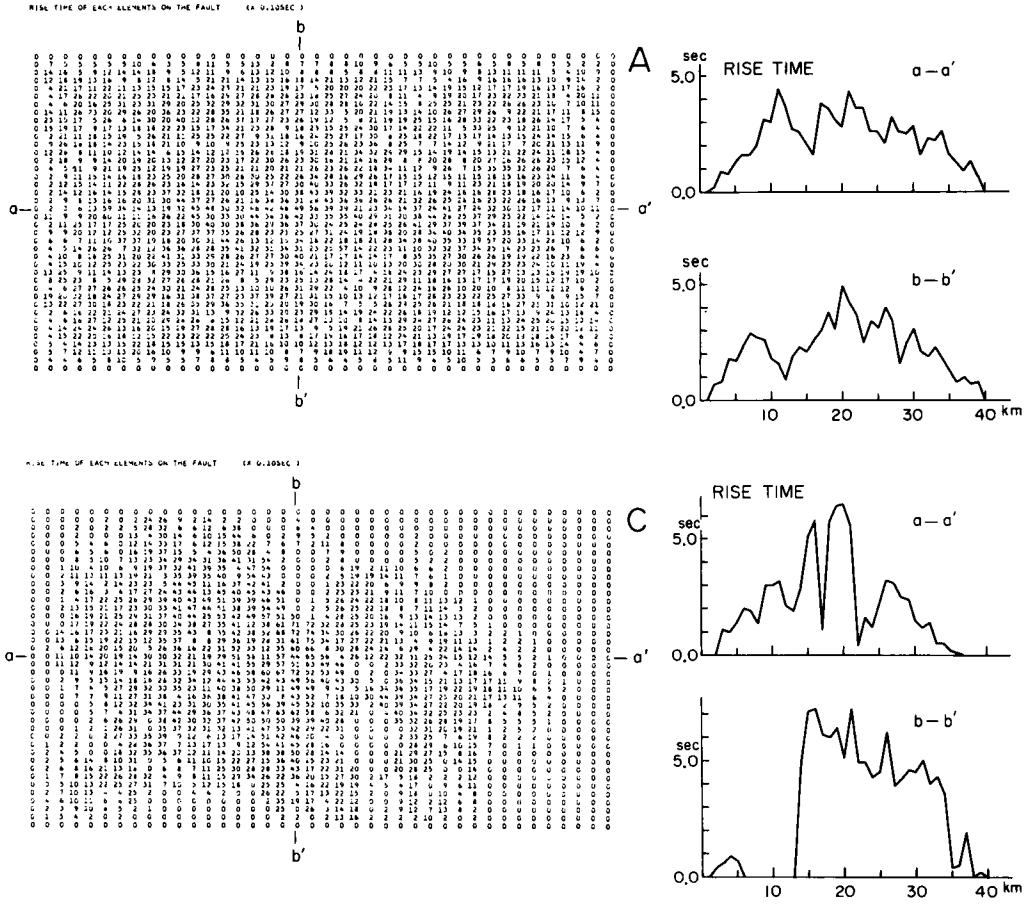


**Figure 7.** Distribution of the rise times on the fault (left) and along the $a$–$a'$ and $b$–$b'$ axes (right) in Cases A and C.

Downloaded from http://gji.oxfordjournals.org/ at Library of Research Reactor Institute, Kyoto University on December 7, 2014

with stronger deviations than in Case A cannot keep such unruptured regions. A most remarkable one is Case C, where we can see very unusual rupture propagation blocked by the existence of large unruptured bays with high strength. This type of irregular propagation often appears in a stochastic percolation model as discussed by Otsuka (1976), but the present results suggest that this is one of the special cases that could arise in the actual rupture process on the fault. Although the rupture pattern as in Case C or Case F2 (not shown here) appears very interesting, we do not claim that this is always the case in the faulting process, since unusually high fracture strength has to be assumed.

Fig. 6 illustrates the displacement-time functions at several selected points on the fault surface in Cases F0, F1 and F2, which have been calculated from equation (8). Case F0 for completely uniform and Case A (not shown here) for weakly non-uniform static frictions show rather smooth curves similar to the ordinary ramp function. Minor fluctuations involved there may be due partly to numerical errors in the finite-difference technique and partly to wave reflections from the upper fixed boundary in the present model, which could be removed by introducing small viscous frictions (Miyatake 1977). It is clearly noticed, however, in other cases that there are a few but remarkable displacement jumps after a flat portion. These step-like displacements suggest that the concerned portion on the fault sticks during a short time and then again slips, depending on the fracture conditions (1)–(3). It is clear that the high non-uniform static frictions on the fault have yielded the above stick–

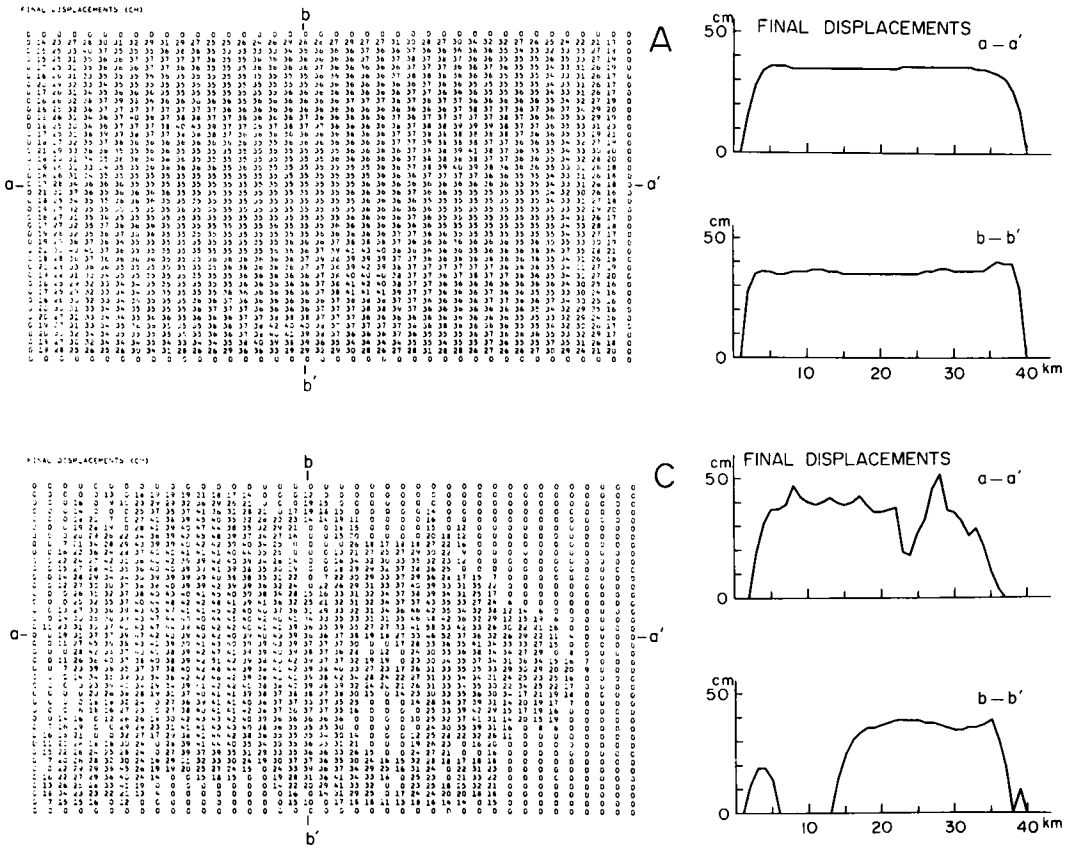


**Figure 8.** Distribution of the final displacements on the fault (left) and along the $a$–$a'$ and $b$–$b'$ axes (right) in Cases A and C.

Downloaded from http://gji.oxfordjournals.org/ at Library of Research Reactor Institute, Kyoto University on December 7, 2014

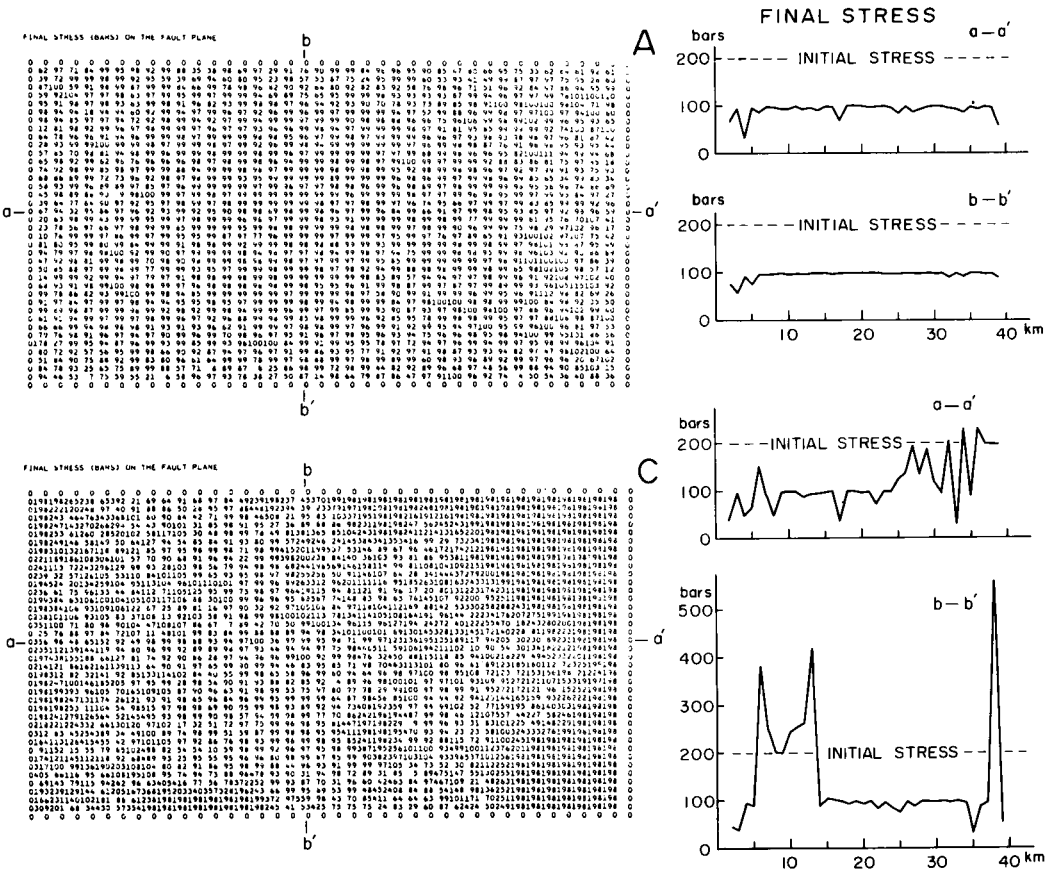


**Figure 9.** Distribution of the final stresses on the fault (left) and along the $a$–$a'$ and $b$–$b'$ axes (right) in Cases A and C. The initial stress level is indicated by broken lines.

slip phenomena as often found in laboratory experiments (e.g. Johnson *et al.* 1973) and as numerically simulated in a one-dimensional model (Ida 1975). This jerky motion could be one source of the generation of high-frequency waves. The distribution of the rise times for attaining the final displacements is shown in the left-hand side of Fig. 7, and the right-hand side gives the distribution along the $a$–$a'$ and $b$–$b'$ axes. It is found that the rise time is longer at the centre of the fault, decreasing towards its edges, although there are considerable variations particularly in Case C. The rise time at the centre in Case C is seen to be longer than in Case A and this may be explained by the difference in the time required to complete the rupture of the fault with different fracture strengths.

Figs 8 and 9 indicate the distribution of the final displacements and stresses remaining after the completion of all rupture process. The right-hand side of the figures show their distribution along the $a$–$a'$ and $b$–$b'$ axes. The final displacements in Case A and also in Case F0 (not shown here) are almost constant except towards the fault edges, where its decreasing trend appears steeper than in two-dimensional calculations. Case C with high frictions, on the other hand, indicates a rather rugged displacement distribution, in which there remain some large unruptured regions that did not slip. Another remarkable feature in this case is that the final slip vectors (not shown here) deviate from the direction of the initial stress to a maximum of 15–20° around the unruptured regions. In Cases F0 and A,

Downloaded from http://gji.oxfordjournals.org/ at Library of Research Reactor Institute, Kyoto University on December 7, 2014

the initial stress drops to the level of dynamic frictional stress at the final stage, and hence the stress drop is almost constant inside the faulted area. It is to be noted, however, that the remnant stress in Case C indicates large variations as shown in Fig. 9, and particularly that there are still high stress concentrations above the initial stress level in and around the unruptured regions. These regions might be regarded as the seismic gap termed 'anti-dislocation' (Andrews 1975), which could produce succeeding earthquakes at a next stage when the stress level again recovers through various processes due to gradual accumulation of tectonic stresses and also by the creep mechanism due to viscoelasticity combined with time-dependent frictions (Dietreich 1972). A similar idea has been suggested by Otsuka (1976) as the source of aftershocks in his stochastic model. If this is indeed the case, the coming aftershocks would have high stress drops due to high stress concentration around the gap, and hence might be large enough to be regarded as independent earthquakes if they occur at sufficient time intervals. This idea may not be unreasonable if large-size geological heterogeneities with unusually high fracture strength are actually distributed on the fault plane. On the other hand, the case of weakly non-uniform strength distribution does not produce such unruptured areas. Rather small variations in the remnant stresses will soon be readjusted probably due to a creep-like recovery process, and hence only small aftershocks would be expected to take place in a relatively short period. This problem is left unanswered at this moment, but will be investigated in the near future.

## 5 Near-field seismic waves

Now we attempt to estimate the ground displacements, synthetic seismograms and their spectra in the near-field, for seismic waves radiated from a variety of the rupture processes on the foregoing frictional fault. The near-field displacements should in principle be calculated by extending the present three-dimensional grid to include the field now in consideration, but it would be practically impossible because of the computer storage required. The alternative adopted here is to replace the calculated displacement-time function at each point on the fault by dynamic dislocations with specific geometry in an infinite medium, and then to calculate the ground displacements at observation sites from the formulations given by Maruyama (1963) and Haskell (1969). This procedure may be allowed when we investigate general features of the waveforms and frequency dependence of the spectrum without detailed analysis into the absolute amplitudes. To attenuate high-frequency noise involved in the source-time function, a three-points moving average at every 0.5 s has been applied to Cases F0, F1 and F2 before doing the above calculations, but not to other cases. Synthetic seismograms are calculated by convolving the ground displacements with the impulse response of the strong-motion seismograph of the JMA type (free period 6 s, damping constant 0.6, magnification 1), and the amplitude spectra are obtained by Fourier-analysis of the seismograms, correcting for the seismograph response. Some examples of the results are described below.

Suppose the case of a vertical fault with dimensions of 20 x 20 km or 40 x 40 km, its upper rim lying just below the ground surface. The initial shear stress is assumed to work left-laterally parallel to the fault. Location of an observation point relative to the fault is specified here by the epicentral distance $\Delta$ from the centre of the fault trace and the azimuth $\phi$ measured clockwise from the direction of the fault trace. Fig. 10 shows the horizontal displacements parallel to the fault plane and the corresponding synthetic seismograms at $\Delta = 20$ km and $\phi = 90^\circ$. Cases F0, F1 and F2 for three different rupture processes give appreciable difference in the waveform, particularly of the relatively short-period components involved. This feature is also obvious in the frequency domain, as shown in the

Downloaded from http://gji.oxfordjournals.org/ at Library of Research Reactor Institute, Kyoto University on December 7, 2014

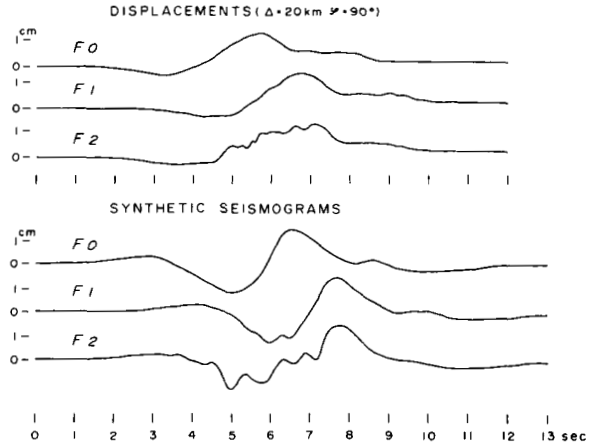


**Figure 10.** Near-field displacements (horizontal component parallel to the fault plane) from frictional faults, Cases F0, F1 and F2, and the corresponding synthetic seismograms at $\Delta = 20$ km and $\phi = 90°$.

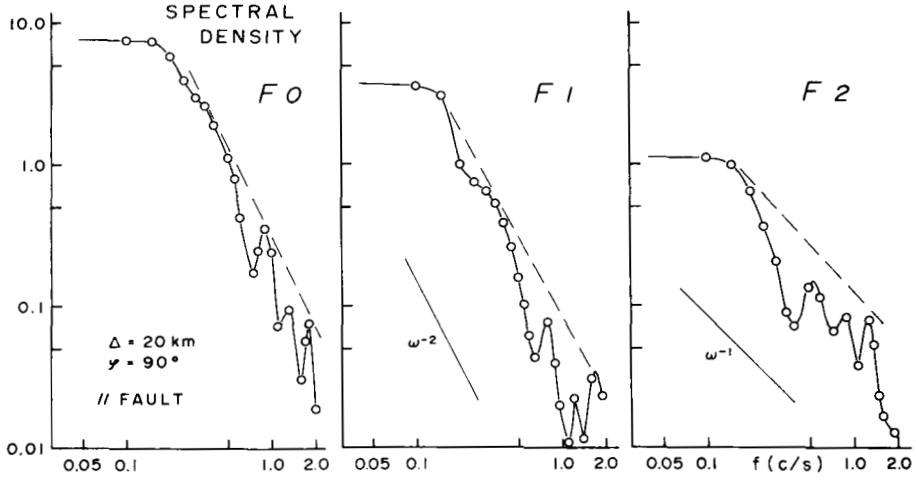


**Figure 11.** Amplitude spectral density of $S$ waves from frictional faults, Cases F0, F1 and F2. The slopes indicated in the figures are proportional to $\omega^{-1}$ and $\omega^{-2}$.

amplitude spectra of $S$ waves in Fig. 11, indicating that the high-frequency asymptote up to 2 c/s appears to be proportional to $\omega^{-1}$ in Case F2 in contrast to $\omega^{-2}$ in Case F0. Since the highest frequency mentioned here corresponds to an $S$ wavelength of 1.6 km, which is greater than three times the grid spacing, we think that the spectra below this frequency may be significant. A similar situation is also clear in Fig. 12(a) and (b) for the synthetic seismograms of the two displacement components parallel and perpendicular to the fault in Case C, which would be observed in several different azimuths at $\Delta = 40$ km. All these seismograms involve much of the high frequencies which predominate between 0.5–1.0 c/s. Frequencies higher than 2 c/s come from noise in the numerical calculations. The amplitude spectra of $S$ waves in these cases are given in Fig. 13, which indicates that the frequency dependence depends on the azimuth with respect to the fault direction. The generation of high-frequency waves with $\omega^{-1}$ dependence coming from strongly non-uniform frictional faults can best be observed in the component perpendicular to the fault (the $X$ component)

Downloaded from http://gji.oxfordjournals.org/ at Library of Research Reactor Institute, Kyoto University on December 7, 2014

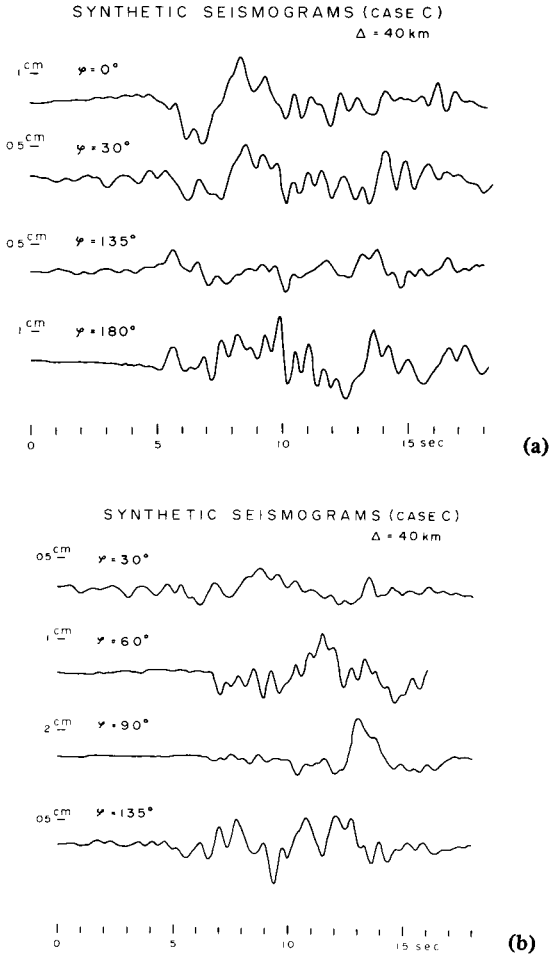


**Figure 12.** Synthetic seismograms in Case C observed at different azimuths at $\Delta = 40$ km. (a) For the displacements perpendicular to the fault plane ($X$ component). (b) For the displacements parallel to the fault plane ($Y$ component).

at $\phi = 0$–$30^\circ$ and $180^\circ$, and in the component parallel to the fault (the $Y$ component) at $\phi = 90^\circ$, since $S$ waves are most effectively radiated into these directions. It is also found that the corner frequencies show some difference depending on the azimuth, and cannot be clearly identified in some cases. This suggests that the frictional faults now in consideration could contaminate and make obscure the corner frequency usually observed.

We next attempt to examine to what extent complex features with short-period waves in the actual records observed in the near-field can be explained by the frictional faulting process just discussed. The uppermost two traces in Fig. 14, given as an example, are the horizontal components of the strong-motion records obtained at the Gifu station ($\Delta = 51$ km, $\phi = 217^\circ$) at the time of the central Gifu earthquake in Japan of 1969 September 9. The records at three other stations involve short-period waves similar to the above records. The fault parameters estimated for this earthquake are: fault dimensions 18 x 10 km, seismic moment $3.5 \times 10^{25}$ dyne cm, average dislocation 64 cm, rise time 1 s and rupture velocity 2.0–2.5 km/s for Model A (Mikumo 1973). The second traces (DSL) in Fig. 14 shows the synthetic seismograms computed from these parameters by the dynamic dislocation theory,



Downloaded from http://gji.oxfordjournals.org/ at Library of Research Reactor Institute, Kyoto University on December 7, 2014

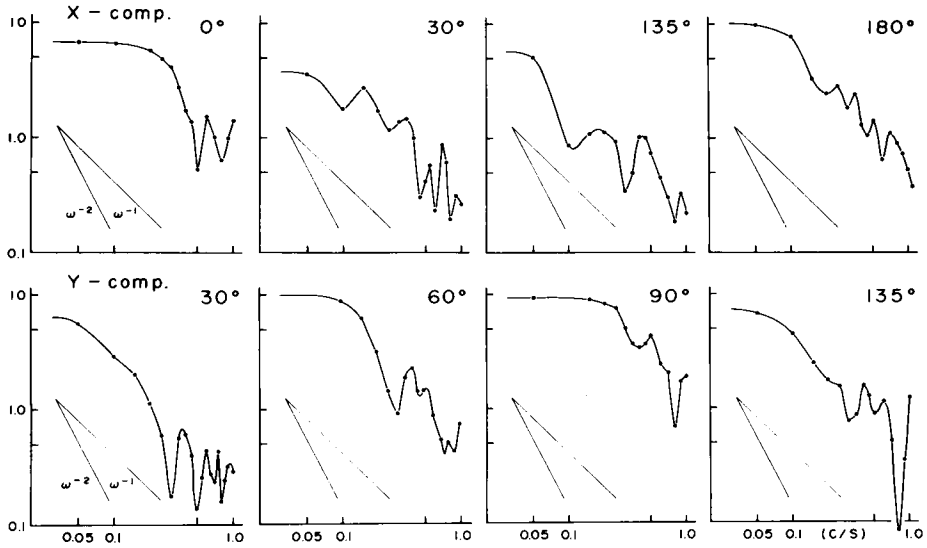


**Figure 13.** Amplitude spectra of *S* waves in Case C observed at different azimuths $\Delta = 40$ km. The slopes indicated in the figure are proportional to $\omega^{-1}$ and $\omega^{-2}$.

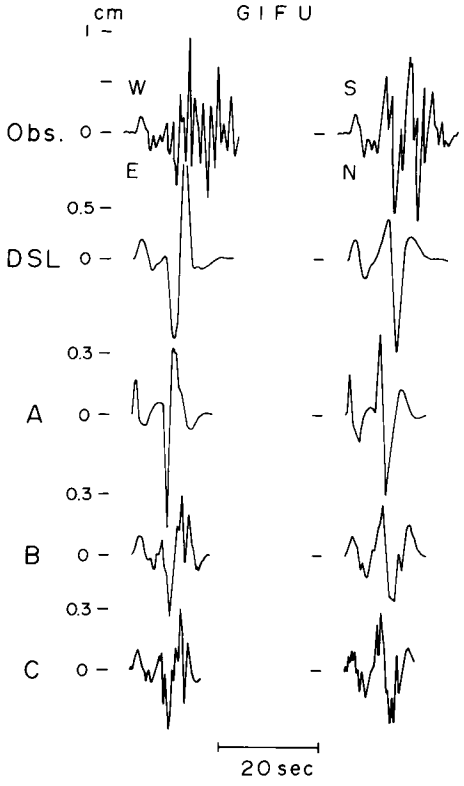


**Figure 14.** Strong-motion records (uppermost traces) observed at the Gifu station ($\Delta = 51$ km, $\phi = 217°$) at the time of the central Gifu earthquake of 1969 September 9, and the corresponding synthetic seismograms. DSL computed from dynamic dislocation model (Mikumo 1973); A, B and C computed from frictional faulting models, Cases A, B2 and C.

Downloaded from http://gji.oxfordjournals.org/ at Library of Research Reactor Institute, Kyoto University on December 7, 2014

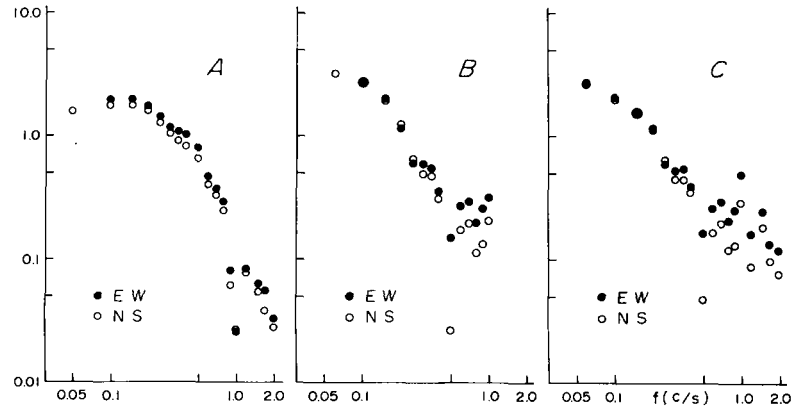


**Figure 15.** Amplitude spectra of *S* waves from frictional faults, Cases A, B2 and C. Solid and open circles are for the EW and NS components, respectively.

which indicate a general agreement in long-period components with the records. The synthetic seismograms calculated from three different frictional faults (Cases A, B and C) with the given fault size and geometry are shown in the next three traces. We notice that Case A gives the waveforms similar to those from the dislocation model while Case C for heavily non-uniform frictions produces short-period components overlapped on relatively long-period waves. Although the direct comparison with the records in the time domain is not so significant because static frictions on the fault are widely distributed in a purely stochastic way, the last traces may well account for the complex features of the observed records. The frequency characteristics of the three different synthetic seismograms are also demonstrated in the amplitude spectra of *S* waves as given in Fig. 15. It is again ascertained that their frequency dependence changes from $\omega^{-2}$ to $\omega^{-1}$ over the high-frequency range as we go from Case A to Case C.

It has been recognized before (Haskell 1964) that the radiation of seismic waves from coherently-propagating dislocation sources over the full length of the fault does not generate total energy and energy spectral density large enough to explain short-period energies experienced in actual observations. To overcome this difficulty, Haskell (1966) introduced a sufficiently small correlation length and correlation time into his statistical model instead of the total fault length and characteristic time. By developing his model, Aki (1967) showed that an exponential decay of the temporal autocorrelation function of dislocation velocity and acceleration leads to the displacement spectral density proportional to $\omega^{-2}$ and $\omega^{-3}$ at high frequencies. It has also been shown (Savage 1972) that the conventional dislocation source gives three linear segments of the far-field displacement spectrum, i.e. $\omega^0$, $\omega^{-1}$ and $\omega^{-2}$ for low, intermediate and high-frequency ranges. This is also the case in Brune's (1970) model. The $\omega^{-1}$ dependence at intermediate frequencies appears only in a limited range for a narrow fault surface in the former model, but in the latter it results from partial release of the effective stress due to premature arrest of slip movements. It is obvious that the above two statistical models as well as narrow dislocation sources do not give full explanation to the observations. Brune's (1970) model assumes a stress applied in a reverse sense shortly after the initial shear stress, but this seems unusual and does not have to be assumed in our present model.

In two-dimensional, unilaterally-propagating antiplane and bilateral in-plane shear cracks over the fault, having a few obstacles with high fracture strength, Das (1976) found that the high-frequency decay of the far-field spectra for both *P* and *S* waves is nearly proportional to

Downloaded from http://gji.oxfordjournals.org/ at Library of Research Reactor Institute, Kyoto University on December 7, 2014

$\omega^{-1}$ to $\omega^{-3/2}$ in and near the direction of rupture propagation but $\omega^{-2}$ in most other cases. She also claimed that the frequency dependence is seriously affected by the arrest mechanism of rupture such as gradual or abrupt stopping. Her results may be compared with our findings in the near-field spectra. In our three-dimensional, frictional fault model, the rupture stops rather abruptly at the fault edges but the stopping effects should be commonly included in all the cases now considered and are not large enough to alter the amplitude-frequency relations.

The most effective factors to generate high-frequency waves are stick–slip faulting and irregular rupture propagation due to non-uniform distribution of static frictions or the fracture strength over the fault surface.

## 6 Conclusions

We have investigated numerically the dynamical rupture process on a three-dimensional frictional fault, where static frictions or the fracture strengths are non-uniformly distributed, being subjected to a finite shear stress. The near-field seismic waves radiated from the fault have also been calculated. The main conclusions obtained are as follows:

(1) If the distributions of the static frictions are completely uniform or weakly non-uniform, the rupture propagates almost elliptically with a nearly *P* wave velocity in the direction parallel to the initial stress, and with a nearly *S* wave velocity in the direction perpendicular to it. The rise time of the displacement function is longer at the centre of the fault than around the fault edges. The final displacements and the remnant stresses are smoothly distributed over the fault.

(2) If static frictions are strongly non-uniform, including the location with unusually high strength, the displacement-time function takes episodically rising forms, suggesting stick–slip-like phenomena. The rupture front shows irregular shapes and its propagation velocity appreciably decreases. In some extreme cases, there remain unruptured areas where high stress concentration takes place. Around these areas, the final slip vectors deviate considerably from the direction of the initial shear stress.

(3) The near-field seismic waves radiated from the frictional faults tend to show complicated waveforms including high frequencies as the heterogeneity of the fracture strength increases. These could give an explanation for high-frequency waves observed in actual strong-motion records near the epicentral region. The amplitude spectra tend to indicate $\omega^{-1}$ frequency dependence in the direction favourable for efficient radiation of *S* waves, in the case of heavily non-uniform distribution of static frictions. The corner frequency could sometimes be contaminated.

## Acknowledgments

We are grateful to Dr Michio Otsuka for many discussions at an early stage of the present study. Helpful suggestions and comments given by Drs Masayuki Kikuchi and Teruo Yamashita are also acknowledged. The senior author benefited from conversations with Dr D. Vére-Jones, Dr James C. Savage and Professor Ralph Lapwood. Our thanks are extended to Mr Y. Hoso for drawing the figures.

Computations involved were made at the Data Processing Center of Kyoto University and at the Computing Room of the Institute for Chemical Research of Kyoto University, Uji.

Downloaded from http://gji.oxfordjournals.org/ at Library of Research Reactor Institute, Kyoto University on December 7, 2014

## References


Aki, K., 1967. Scaling law of seismic spectrum, *J. geophys. Res.*, **72**, 1217–1231.

Aki, K., 1968. Seismic displacements near a fault, *J. geophys. Res.*, **73**, 5359–5376.

Andrews, D. J., 1975. From antimoment to moment: plane-strain models of earthquakes that stop, *Bull. seism. Soc. Am.*, **65**, 163–182.

Andrews, D. J., 1976. Rupture velocity of plane strain shear cracks, *J. geophys. Res.*, **81**, 5679–5687.

Brace, W. F. & Byerlee, J. D., 1966. Stick–slip as a mechanism for earthquakes, *Science*, **153**, 990–992.

Brace, W. F., 1972. Laboratory studies of stick–slip and their applications to earthquakes, *Tectonophys.*, **14**, 189–200.

Brune, J. N., 1970. Tectonic stress and the spectra of seismic shear waves from earthquakes, *J. geophys. Res.*, **75**, 4997–5009.

Burridge, R., 1969. The numerical solution of certain integral equations with non-integrable kernels arising in the theory of crack propagation and elastic wave diffraction, *Phil. Trans. R. Soc. Lond. A*, **265**, 353–381.

Burridge, R., 1973. Admissible speeds for plane-strain self-similar cracks with friction but lacking cohesion, *Geophys. J. R. astr. Soc.*, **35**, 439–455.

Burridge, R. & Knopoff, L., 1967. Model and theoretical seismology, *Bull. seism. Soc. Am.*, **57**, 341–371.

Burridge, R. & Halliday, G. S., 1971. Dynamic shear cracks with friction as models for shallow focus earthquakes, *Geophys. J. R. astr. Soc.*, **25**, 261–283.

Byerlee, J. D., 1970. The mechanics of stick–slip, *Tectonophys.*, **9**, 475–486.

Das, S., 1976. A numerical study of rupture propagation and earthquake source mechanism, *PhD thesis*, Massachusetts Institute of Technology.

Dietreich, J. H., 1972. Time-dependent friction as a possible mechanism for aftershocks, *J. geophys. Res.*, **77**, 3771–3781.

Dietreich, J. H., 1973. A deterministic near-field source model, *Proc. 5th Conf. Earthq. Eng.*, Rome, Italy.

Fossum, A. F. & Freund, L. B., 1975. Non-uniformly moving shear crack model of a shallow focus earthquake mechanism, *J. geophys. Res.*, **80**, 3343–3347.

Hanson, M. E., Sanford, A. R. & Shaffer, R. J., 1971. A source function for a dynamic bilateral brittle shear fracture, *J. geophys. Res.*, **76**, 3375–3383.

Hanson, M. E., Sanford, A. R. & Shaffer, R. J., 1974. A source function for a dynamic brittle unilateral shear fracture, *Geophys. J. R. astr. Soc.*, **38**, 365–376.

Haskell, N., 1964. Total energy and energy spectral density of elastic wave radiation from propagating faults, *Bull. seism. Soc. Am.*, **54**, 1811–1842.

Haskell, N., 1966. Total energy and energy spectral density of elastic wave radiation from propagating faults, 2. A statistical source model, *Bull. seism. Soc. Am.*, **56**, 125–140.

Haskell, N., 1969. Elastic displacements in the near-field of a propagating fault, *Bull seism. Soc. Am.*, **59**, 865–908.

Husseini, M. I., Jovanovich, M. J., Randall, M. J. & Freund, L. B., 1975. The fracture energy of earthquakes, *Geophys. J. R. astr. Soc.*, **43**, 367–385.

Ida, Y. & Aki, K., 1972. Seismic source time function of propagating longitudinal shear cracks, *J. geophys. Res.*, **77**, 2034–2044.

Ida, Y., 1973. Stress concentration and unsteady propagation of longitudinal shear cracks, *J. geophys. Res.*, **78**, 3418–3429.

Ida, Y., 1975. Analysis of stick–slip and earthquake mechanism, *Phys. Earth planet. Int.*, **11**, 147–156.

Johnson, T., Wu, F. & Scholz, C. H., 1973. Source parameters for stick–slip and for earthquakes, *Science*, **179**, 278–279.

Knopoff, L., Mouton, J. O. & Burridge, R., 1973. The dynamics of a one-dimensional fault in the presence of friction, *Geophys. J. R. astr. Soc.*, **35**, 169–184.

Kostrov, B. V., 1966. Unsteady propagation of longitudinal shear cracks, *J. Appl. Math. Mech.*, **30**, 1241–1248.

Madariaga, R., 1976. Dynamics of an expanding circular fault, *Bull. seism. Soc. Am.*, **66**, 639–666.

Maruyama, T., 1963. On the force equivalents of dynamic dislocations with reference to the earthquake mechanism, *Bull. Earthq. Res., Inst.*, **41**, 467–486.

Mikumo, T., 1973. Faulting mechanism of the Gifu earthquake of September 9, 1969, and some related problems, *J. Phys. Earth*, **21**, 191–212.

Miyatake, T., 1977. Numerical simulation of dynamical faulting process, (in Japanese), *ZISIN, Ser. II*, **30**, in press.

Ohnaka, M., 1973. A physical understanding of the earthquake source mechanism, *J. Phys. Earth*, **21**, 39–53.


Downloaded from http://gji.oxfordjournals.org/ at Library of Research Reactor Institute, Kyoto University on December 7, 2014

Otsuka, M., 1971. A simulation of the earthquake occurrence, Part 1. A mechanical model, (in Japanese), *ZISIN, Ser. II,* **24**, 13–25.

Otsuka, M., 1976. A simulation of earthquake occurrence, Part 5. An interpretation of aftershock phenomena, (in Japanese), *ZISIN, Ser. II,* **29**, 137–146.

Richards, P., 1976. Dynamic motions near an earthquake fault: a three-dimensional solution, *Bull. seism. Soc. Am.,* **66**, 1–32.

Savage, J. C., 1972. Relation of corner frequency to fault dimensions, *J. geophys. Res.,* 77, 3788–3795.

Takeuchi, H. & Kikuchi, M., 1973. A dynamical model of crack propagation, *J. Phys. Earth,* **21**, 27–37.

Yamashita, T., 1976. On the dynamical process of fault motion in the presence of friction and inhomogeneous initial stress, Part 1. Rupture propagation, *J. Phys. Earth,* **24**, 417–444.

Downloaded from http://gji.oxfordjournals.org/ at Library of Research Reactor Institute, Kyoto University on December 7, 2014